Neotectonic evolution of Northeastern Venezuela . Geomorphological and seismic analysis in the Monagas Fold and Thrust Belt

Atiria Fajardo, Charles Aubourg, Bertrand Nivière, Vincent Regard, Redescal Uzcátegui

Neotectonic evolution of Northeastern Venezuela Basin. Geomorphological and seismic analysis in the Monagas Fold and Thrust Belt

Atiria Fajardo[a]*, Charles Aubourg[b], Bertrand Niviere[b], Vincent Regard[c], Redescal Uzcátegui[d]

[a] Geohidra Consultores, C.A., Caracas, Venezuela. fajardoaq@gmail.com.
[b] Université de Pau et des Pays de l'Adour, E2S UPPA, CNRS, TOTAL, LFCR, Pau, France. charles.aubourg@univ-pau.fr, bertrand.niviere@univ-pau.fr.
[c] GET (Géosciences Environnement Toulouse), University of Toulouse, UPS (OMP), CNRS, IRD, CNES, Toulouse, France. vincent.regard@get.omp.eu.
[d] Universidad Simón Bolívar, Caracas, Venezuela. ruzcategui@usb.ve.

Abstract

In Northeastern Venezuela, since 10 Ma, the tectonic setting is dominated by the eastward translation of the Caribbean Plate accommodated mainly by the E-W El Pilar strike-slip fault. However, to the south, in the Monagas Fold and Thrust Belt (MFTB), evidence of active compression has been identified in the southern limit of the Urica dextral fault. The objective of this study is to integrate geomorphological, dating terraces and 2D-3D seismic data in four zones of the MFTB: Tarragona, Punta de Mata, Jusepín, and Amarilis to understand the tectonics relationship between surficial and deep deformation in the area. These zones show surface deformations such as topographic uplifts, tilted, folded and faulted terraces, and drainage anomalies.

The age of the river terraces obtained through ^{10}Be and ^{26}Al methods indicates that these terraces were formed in the late Pleistocene. The oldest terrace, located in the Tarragona zone, has a maximum exposure age of 90±5 ka and the youngest, located in the Punta de Mata zone of 15±5 ka. Additionally, we calculated an uplift rate of 0.3-0.4 mm/y for Plio-Pleistocene units using the deformation of the Late Miocene Unconformity (LMU). This rate coincides with the vertical deformation rate average calculated from terraces dating, which suggests that the deformation rate in the MFTB has not changed significantly for the last 5.3 Ma.

The ridges observed at the surface and the structural highs interpreted from seismic sections indicate that the uplifting has been active up to the present through the activation of deep thrusts. We propose that the deformation on the surface is linked to the Tarragona, Pirital, Furrial thrusts, and the Amarilis backthrust activity and the youngest thrusts developed in the Carapita Formation. However, this surface deformation

decreases towards the SSE away from the Urica fault; therefore, the neotectonic deformation is believed to be caused by the horsetail termination activity at the southern limit of the Urica fault.

Keywords: Urica, Pirital, Furrial, horsetail termination, cosmogenic nuclides, terraces.

1. Introduction

The breakup of Pangea during Jurassic times caused the beginning of the divergence between the North and South American plates (Summa et al., 2003). It led to the formation of the Caribbean crust between both plates from 80 to 30 Ma according to some authors (Ball et al., 1969; Aubouin et al., 1982; Sykes et al., 1982; Donnelly, 1985; Frisch et al., 1992; all these in Meschede & Frisch, 1998) or in the Pacific domain during the late Mesozoic for others (Stephan et al., 1982; Pindell and Barrett, 1990; Babb and Mann, 1999, among others). Since the Oligocene, in Northeastern Venezuela, the oblique collision between the Caribbean and South American plates formed the Serranía Del Interior (SDI), the Monagas Fold and Trust Belt (MFTB) and the Maturín sub-Basin (Fig. 1). During the last 10 Ma, the eastward translation controls the neotectonic activity in the area, which mainly accommodated by the El Pilar dextral fault (Algar and Pindell, 1993; Pindell et al., 1998).

In the MFTB, active faulting and recent deformations are less intense than the ongoing activity along the El Pilar fault that accommodated the main slip between the South American and Caribbean plates (Fig. 1). Northeast of the MFTB, Wagner (2004) identified in the field, deformed terraces in the piedmont of the SDI, although satellite imagery and DEM resolution are poorly informative in this area due to vegetation and cloud covers. Additionally, active tectonics close to MFTB have been studied by the Fundación Venezolana de Investigaciones Sismológicas (FUNVISIS) through geodetic, palaeoseismic, seismic data, focal mechanisms (Beltrán et al., 1996; Singer et al., 1998; Audemard et al., 2005; Audemard, 2000, 2006, 2011) and GPS studies (Jouanne et al., 2011; Reinoza et al., 2015). All data evidenced active tectonics within Northeast Venezuela (Fig.1). Eclipsed by the strongly active and seismogenic the El Pilar fault, the Neogene tectonic stage has been less studied in the southern slope of these ranges (e.g., Zinck and Urriola, 1970; Singer et al., 1998; Audemard et al., 2005; among others). Moreover, hydrocarbon potential in the Maturín sub-Basin has motivated many geological interpretations where the cross-sections show folding of late Miocene sequences and unconformities, specifically in the MFTB (Fig. 1).

The main motivation of this study is to improve the knowledge about mechanisms that produce recent deformation in the MFTB. For this purpose, we related subsurface and surface deformation using geomorphic field evidence and seismic analysis in the MFTB based on; (1) morphotectonic analysis (2) terraces dating through cosmogenic ^{10}Be and ^{26}Al analyses (3) description of deep and near-surface structures using 2D and 3D seismic data and (4) calculation of vertical deformation and uplift rate using terrace ages and seismic interpretation. Finally, we propose a regional structural evolution of the active deformation in the area since 10 Ma to the present day.

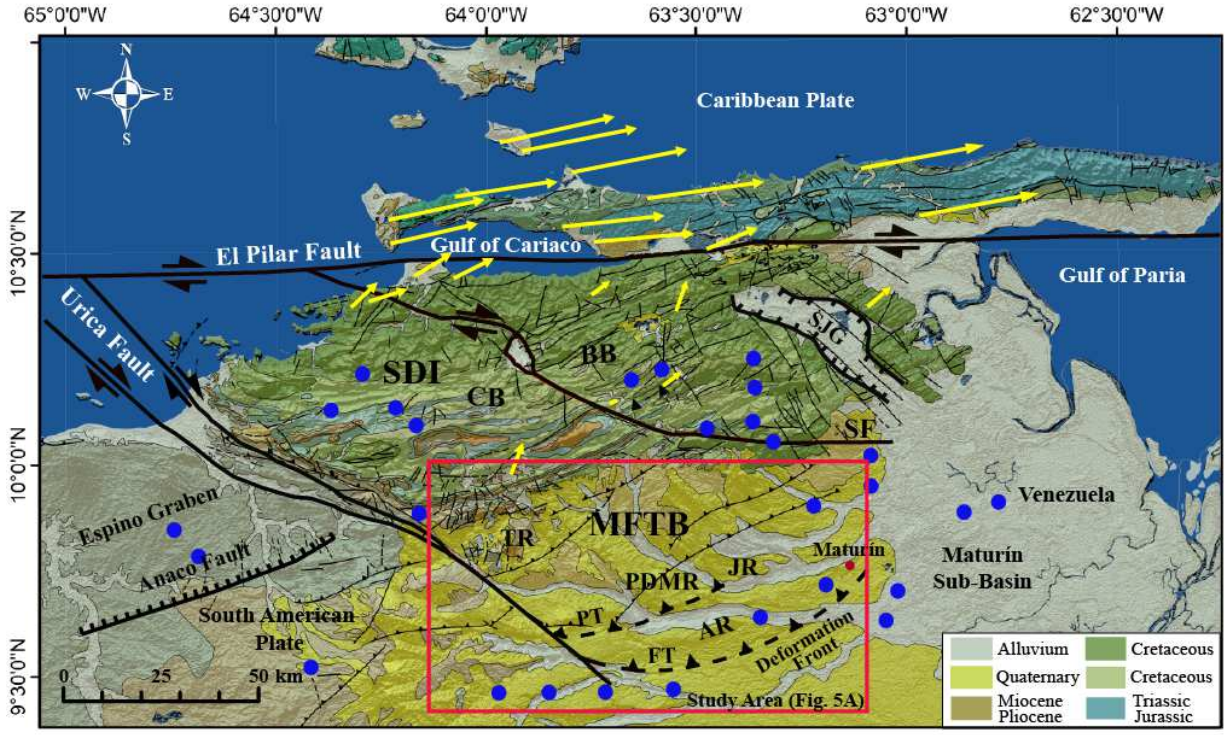

Fig. 1. Tectonic and geological map of Northeastern Venezuela, showing the structural features and the study area location (Modified from Urbani et al., 2005). SDI: Serranía Del Interior; CB: Caripe Block; BB: Bergantín Block; SF: San Francisco Fault; MFTB: Monagas Fault Thrust Belt; PT: Pirital Thrust; FT: Furrial Thrust; TR: Tarragona Ridge; PDMR: Punta de Mata Ridge; AR: Amarilis Ridge; JR: Jusepín Ridge; SJG: San Juan Graben. Blue circles: selected seismic events magnitude 3.0-3.9 (FUNVISIS, 2020). Yellow arrows: Velocities observed by Global Navigation Satellite System (GNSS) campaign measurement (from Jouanne et al., 2011).

2. Geological setting

Since the Oligocene, the interaction between the Caribbean and South American plates has produced the active margin in Northeastern Venezuela Basin (Mann et al., 1990). In the middle Miocene, the northern boundary

of South America was affected by the migration of the Caribbean Plate, eastward defined as a diachronous transpressive movement (Pindell and Barrett, 1990; Ave Lallemant, 1997; Pindell and Kennan, 2009). This transpression movement interpreted as a strain partitioning system, accommodated by a northern region of strike-slip deformation and a southern region of fold-thrust belt contraction (Lingrey, 2007). This fold-thrust belt system crops out in Eastern Venezuela in the SDI hinterland and the MFTB foothill (Fig. 1).

The MFTB is the study area of this work. This province is the transition between the uplifted and strongly shortened SDI to the north and the Maturín sub-Basin to the south (e.g., Jácome et al., 2003). The Pirital and the Furrial thrusts are de main structural features present in the area (Fig. 1). The Pirital thrust is considered by some authors the southern boundary of the SDI (e.g., Parnaud et al., 1995; Duerto, 2007) and its orientation NE-SW differs to the overall E-W trend of the thrust system, possibly indicating an out-of-sequence event (e.g., Parnaud et al., 1995; Parra et al., 2011). This thrust is active since the late Oligocene-early Miocene and seems to be diachronous from west to east. At the middle Miocene the Pirital thrust developed a frontal high-angle ramp during an out-of-sequence phase possibly localized above an earlier normal fault (Parra et al., 2011), it accommodated a shortening of 80 km (Parnaud et al., 1995) with a horizontal displacement of 20-30 km and a vertical displacement 4-5 km (Di Croce, 1999). In a more distal position, the Furrial thrust runs parallel to the Pirital thrust but only affecting post-early Cretaceous units, and it could have accommodated 17-20 km of slip (Márquez et al., 2003; Fig. 1). Its configuration varies along-strike being more complex towards the west (Parra et al., 2011).

Two regional unconformities have been identified in the MFTB: the Middle Miocene Unconformity (MMU) with an average age of 12.5 Ma based on stratigraphic correlations, and the Late Miocene Unconformity (LMU) interpreted as an important hiatus with an age of 5.3 Ma (Sztrakos and Medina, unpublished results cited in Parra et al., 2011). The MMU is an erosional surface defined as the base of the La Pica Formation (Fig. 2). It truncates the units below and the Furrial and Pirital thrusts. Thrust activity in the area has been deforming the post-late Miocene sediments, including the MMU (Fig. 2). The LMU defines the base of the Pliocene sediments represented by the La Mesa/Las Piedras Formation and extends from the Pirital thrust sheet to the south of Furrial thrust sheet (Parra et al., 2011).

Since the late Miocene, the movement vector of the Caribbean plate with respect to the Central Range of Trinidad has N086º ± 2ºN direction, and N084º ± 2ºE direction with respect to South America according to GPS data (Weber et al., 2001; Pérez et al., 2001). These movement vectors suggest an almost pure wrenching movement with a slight transtension in eastern Venezuela (Audemard et al., 2006). At present, GPS shows that

the El Pilar fault would concentrate the relative displacement between the Caribbean and South America plates, with a pure dextral strike-slip movement and an insignificant shortening across the SDI thrusts (Jouanne et al., 2011). However, Audemard et al. (2006) suggest that a compressive component is always running and caused uplift and important positive relief features in part of the Eastern Venezuelan Coastal and Interior ranges (Fig. 1). Moreover, Fajardo (2015) proposes that this dextral displacement has developed a synthetic Riedel shear with clockwise block rotation in the SDI where part of this movement is being accommodated southwards in the MFTB.

In Northeastern Venezuela the seismicity is mainly concentrated in the plate boundary around the El Pilar fault reaching earthquakes >5 in magnitude. However, in the SDI seismic events occur mainly near the Urica and San Francisco right-lateral strike-slip faults (FUNVISIS, 2020). Further south along the MFTB, seismic activity is weaker than in the SDI, and the events are localized mainly along the WSW-ENE oriented deformation front (Fig. 1). This ongoing activity in the MFTB is currently expressed by river terraces and Pleistocene age deformations. Zinck and Urriola (1970) recognized four river terraces along the Guarapiche River. They found asymmetric grabens characterized by staggered step series, these grabens are bounded by scarps of 5 - 10 m high, southerly, and in the Tonoro River, they observed three river terrace levels. In the northeast of the MFTB, Wagner (2004) identified four stepped river terrace levels across the Jusepín thrust and interpreted them as fold related to deep fault.

The La Mesa Formation capped the region, and is composed of siliceous coarse sands, gravels with very hard ferruginous cement, red almost black conglomerates, yellowish-white sands and red-purple sands (Fig. 2). This Formation also contains discontinuous lenses of sandy clay and silts (González de Juana et al., 1980). The thickness is highly variable, but generally decreases from north to south, due to changes in the fluvial-deltaic sedimentation, and increases from west to east due to the advance of deltaic sediments (González de Juana et al., 1980). The La Mesa Formation is considered of Pleistocene age based on the transitional relation with the Pliocene Las Piedras Formation (Zinck and Urriola, 1970; LEV, 1997).

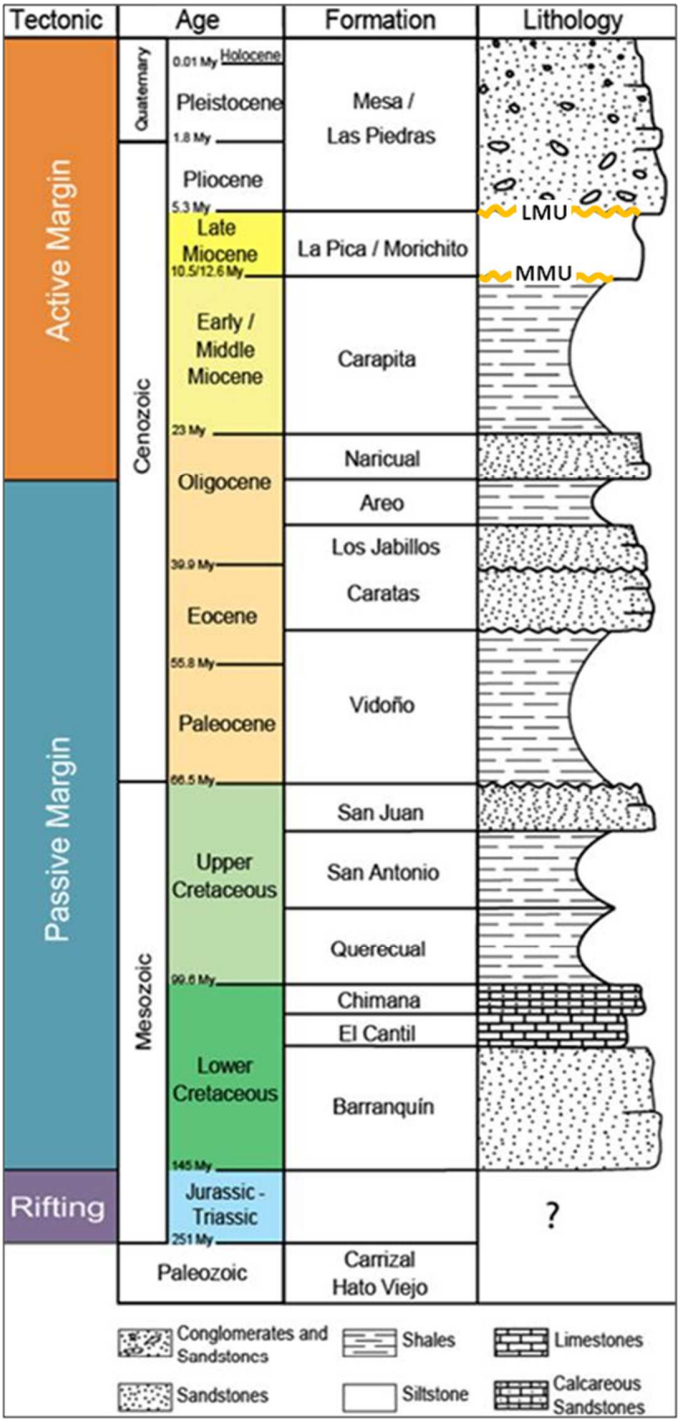

Fig. 2. Stratigraphic chart of Northeastern Venezuela Basin showing the stratigraphic units and unconformities interpreted on seismic sections. Modified from Parra et al. (2011)

3. Methods

3.1. Topographic analysis and fieldwork

The aim of this analysis was to construct a morpho-structural model. We used a Digital Elevation Model (DEM) with a 90 m resolution, aerial photos, and orthophotos (1:5000 scale), and interpreted drainage networks and geomorphic features as river terraces using ArcGIS and ENVI software. We also generated topographic profiles to identify evidence of deformation as scarps, slopes and drainage anomalies. This model was validated with field data such as tilts, folds and faults in river terraces and ridges.

3.2. Dating terraces from ^{10}Be and ^{26}Al cosmogenic nuclides method

To obtain the exposure age of terraces in the MFTB, we used the ^{10}Be and ^{26}Al cosmogenic nuclides method (Figs. 3 and 4). This method is useful to quantify terrace ages by sampling rocks at their surface, making the assumption that when they deposited their cosmogenic nuclide content was negligible, which is generally true (e.g., Nishiizumi et al.,1986; Klein et al., 1986). In the MFTB, we collected sampled rocks from five terraces distributed in the area (3S, 4S, 6S, 9S and 12S, see Fig. 5A). These samples are mainly composed by quartz, similar in size and shape, and are neither fractured nor weathered. We collected them only where they were embedded within the surface terrace, and in flat areas, distant from escarpments and landslides, to avoid collecting samples transported and, or eroded from neighboring areas. We took three or two samples from each terrace to better discriminate complex exposure histories. There might be a discrepancy between ^{26}Al and ^{10}Be ages, this discrepancy comes from inheritance which itself was due to a burial episode.

We investigated the possible sample histories through time to constrain the terrace ages, for this, we assumed a history in three phases. During the first phase, the rock was exhumed with an initial denudation rate (e) and at an initial production (P_alt) calculated according to the upstream average altitude of ~1200 m (average altitude of the SDI mountains). In the second phase, the rock was transported from the mountain and stored within an alluvial deposit to a significant depth ($z > 10$m; we took $z = 100$m in calculations) and during a storage time (burial) ranging from ~ 0 to 5.3 Ma, we propose here that during burial, the ^{26}Al/^{10}Be ratio decreases following radioactive decay. Finally, during the third phase, the rock was abruptly removed from the alluvial surface as a result of incision by the river and/or tectonic movements and re-deposited on the terrace sampled.

To calculate the vertical deformation rate, we divided the vertical offset observed in each deformed terraces by its exposure age obtained by ^{10}Be and ^{26}Al dating (Table 2). In all cases, we assumed that the vertical offset was produced after exposure of the terrace. The rate was calculated in terraces where visible deformations as folding or scarps were observed in the fieldwork, DEM and/or aerial photos.

3.3. Seismic Interpretation

The seismic interpretation was based on 1200 km of 2D time-migrated seismic lines, 980 km^2 of 3D seismic data depth migrated, and twelve key wells distributed around the MFTB. Key wells contain stratigraphic data, well logs, and time/depth tables for seismic data calibration. All the seismic and well data was acquired by Petróleos de Venezuela (PDVSA). The interpretation was focused mainly in structure identification such as unconformities, structural highs, thrusts, and faults, based on stratigraphic markers interpreted and validated by the PDVSA multidisciplinary team, which has been working in the area for a long time (e.g., DiCroce et al., 1999; Duerto, 2007; Parra et al., 2010; Sánchez et al., 2010). 2D seismic interpretation was carried out in several zones of the area, but in this paper, we only show the seismic lines located across the surfaces structures described in the geomorphological study: seismic line M1 across the Tarragona high and lines M2, M3, M4, and M5 across the Amarilis, Punta de Mata and Jusepín highs (Fig. 7A)

To quantify the uplift rate and shortening in the Plio-Pleistocene units, we took the LMU geometry as a reference assuming that 5.3 Ma ago it was horizontal, so the vertical offset will be the difference in depth between the LMU horizon and the top of the Plio-Pleistocene units. Then, the uplift rate is calculated dividing the vertical offset by the LMU age (5.3 Ma); this result is an average rate for the last 5.3 Ma. To obtain the shortening, we calculated the change in length between the undeformed and deformed LMU horizon. This procedure was reproduced in several lines, evenly distributed in the 3D seismic block.

4. Results

4.1. Exposure age calculations from ^{10}Be and ^{26}Al cosmogenic nuclides method

Cosmogenic nuclide concentrations range obtained in this study vary between 50-950 kat/g and 300-5000 kat/g for ^{10}Be and ^{26}Al, respectively. The ^{26}Al/^{10}Be ratios are low, ranging 2.5-5.9 (Table 1). The estimation of the exposure ages was carried out using the production schemes of Desilets et al., (2006); Dunai (2001); Lifton et al., (2005); Lal (1991); and Stone (2000). However, we decided to consider only the ages obtained from the production scheme of Dunai (2001) due to the alternative production scheme, not leading to significantly different results in samples from the same site. Moreover, we observed discrepancies between ^{26}Al and ^{10}Be ages; commonly the age discrepancy comes from inheritance, which itself was due to a burial episode. The concentration results show two episodes, burial followed by re-exposure at the terrace surface (Fig. 3); as a consequence, the burial duration evaluation is a minimum estimate. This diagram also shows that the evolution of samples 4SA, 9SC, 9SA, 9SB, 12SB, and 12SB can be explained by a burial time between 1 and 2 Ma maximum. Samples 3SA, 3SC, 6SA, and 6SC can be related to a history with a burial time of ~500 ka.

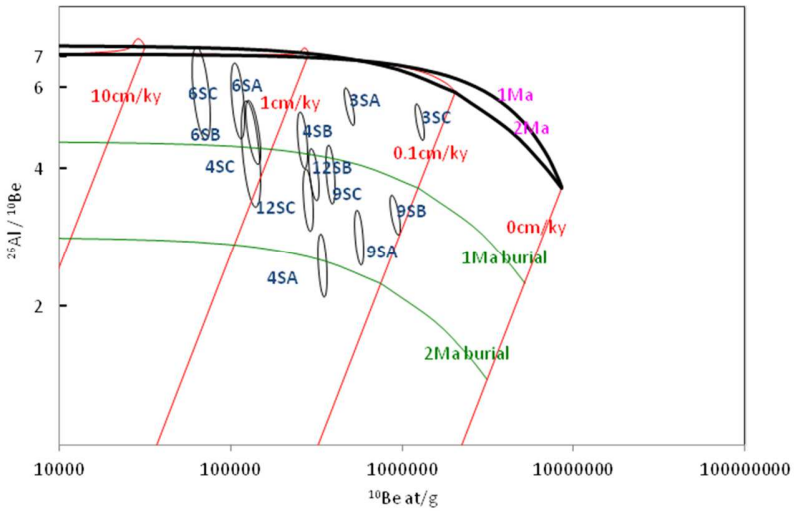

Fig. 3. 'Banana' of ^{26}Al and ^{10}Be concentrations for the terraces sampled (from Vermeesch, 2007). Bold lines represent the concentration of superficial samples (one is for erosion only, the other for denudation only). Most samples are below the bold lines, which indicate a complex history with an integrated storage period. This graph does not consider the sample history after burial when exposed at the terrace surface, whose main effect is an increase in ^{26}Al/^{10}Be.

Knowing that the samples have a history with a maximum burial time of 2 Ma, we calculated two additional evolution time models to constrain the ages obtained by the dating methods: a model for a burial time limit of 1 and 2 Ma. In the following, two examples are explained in the graph (Fig. 4). In the case of sample 9SB, if

we postulate a burial of T=2 Ma, this sample needs Θ=40 ka of exposure to explain its ^{26}Al and ^{10}Be content; it therefore, originates from a mountain eroding at a rate of e=5.10^{-6} m/y; it cannot be explained for T=1 Ma burial, because its current ^{26}Al /^{10}Be ratio is too low. For sample 12SB, the concentration can be explained by a 1Ma-burial without further exposure or by a 2Ma-burial followed by a Θ=30 ka exposure; in both cases, the initial denudation rate is approximately 2-3.10^{-5} m/y. Finally, Table 1 shows the exposure ages calculated for each site after applying the evolution time models.

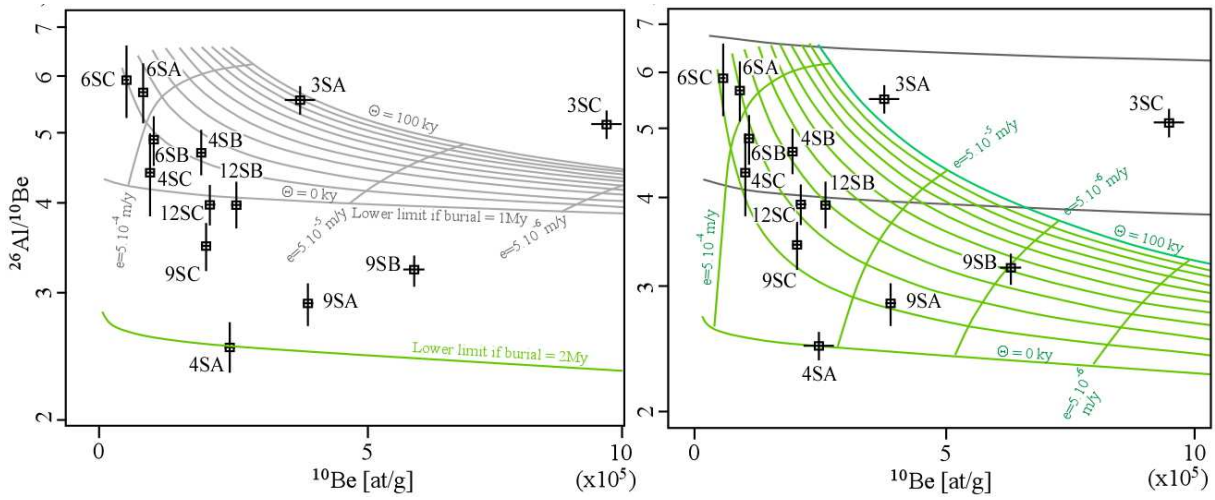

Fig. 4. Evolution model through time for samples stored between 1 Ma (left) and 2 Ma (right). The curves display expected cosmogenic nuclides concentrations for a final stated (Θ) between 0 and 100 ka at the terrace surface.

Table 1. ^{10}Be and ^{26}Al results following production scheme of Dunai (2001) from Cronus web calculator v2.0.

Site	Sample	Latitude (N)	Longitude (W)	Elevation (m)	^{10}Be concentration (10^5 at/g)	^{26}Al concentration (10^5 at/g)	^{10}Be age (ka)	^{26}Al age (ka)	^{26}Al / ^{10}Be ratio (at/g)	Estimated Age (ka)
3S (Tarragona)	3SA	9°43'48"	64°00'07"	287	3.7 ± 0.1	20.5 ± 0.6	103.0 ± 12.9	87.2 ± 11.1	5.5 ± 0.3	90 ± 5
	3SC				9.4 ± 0.3	47.8 ± 1.6	267.2 ± 34.7	207.2 ± 28	5.1 ± 0.2	
4S (Punta de Mata)	4SA	9°44'14"	63°32'20"	204	2.4 ± 0.1	6.0 ± 0.4	71.7 ± 11	28.0 ± 3.9	2.5 ± 0.2	15 ± 5
	4SB				1.9 ± 0.1	8.8 ± 0.6	55.7 ± 8.9	39.1 ± 5.3	4.6 ± 0.3	
	4SC				1.0 ± 0.1	4.2 ± 0.5	29.6 ± 4.0	19.8 ± 3.3	4.3 ± 0.6	
6S (Punta de Mata)	6SA	9°45'03"	63°39'23"	265	0.8 ± 0.0	4.7 ± 0.4	25.1 ± 3.2	21.5 ± 3.1	5.6 ± 0.5	14 ± 5
	6SB				1.0 ± 0.1	4.9 ± 0.3	30.1 ± 3.9	22.4 ± 3.0	4.8 ± 0.4	
	6SC				0.5 ± 0.0	3.0 ± 0.3	15.8 ± 2.1	14.0 ± 2.2	5.9 ± 0.7	
9S (Amarilis)	9SA	9°36'42"	63°36'52"	175	3.9 ± 0.1	11.0 ± 0.7	114.7± 14.4	48.6 ± 6.6	2.8 ± 0.2	25 ± 5
	9SB				6.3± 0.2	20.0 ± 0.8	189.5 ± 24.2	92.6 ± 12.0	3.2 ± 0.2	
	9SC				2.0 ± 0.1	6.8 ± 0.5	60.2 ± 7.5	32.1 ± 4.5	3.4 ± 0.3	
12S (Jusepín)	12SB	9°44'19"	63°26'52"	95	2.6 ± 0.1	10.0 ± 0.7	82.6 ± 10.3	47.0 ± 6.5	3.9 ± 0.3	35 ± 5
	12SC				2.1 ± 0.1	8.0 ± 0.4	65.0 ± 8.2	38.8 ± 5.1	3.9 ± 0.3	

4.2. Quaternary deformation in the MFTB

4.2.1 Quaternary deformation in the Tarragona ridge

In the Tarragona ridge, we describe a terrace remnant ("3S" on Fig. 5A). The outcrop is topped by a ~0.5 m thick alluvial layer made of small pebbles located above coarse sands (Fig. 6A). The terrace dips more than 15° towards the SW. Under the alluvium layer, a yellowish siltstone layer lays below a greenish one. The greenish silts at the NE; (right in Fig. 6A) have been displaced and placed in contact with the yellowish silts at the SW; (left in Fig. 6A). The geometry of the contact suggests the presence of a ~10° north dipping reverse fault that displaced the siltstones and tilted the overlain alluvium layer. However, we did not observe any clear evidence of a surface rupture at the outcrop, and we cannot rule out here the hypothesis of a simple sedimentary relationship. But this unconformity implies that the silts have been tilted, and the slope of the basal surface of the alluvium at the top is far too strong to be depositional. This morphology, therefore, requires a tilting after the deposit of these alluviums, tilting orchestrated by a fault which, if it does not necessarily emerge, is not far from doing so. So this observation can be interpreted as a surface faulting associated with the Tarragona thrust. According to ^{10}Be and ^{26}Al results, samples 3SA and 3SC can be related to a moderate burial duration of ~500 ka and then re-exhumation. The exposure age calculated for this site was ~90 ka.

4.2.2 Quaternary deformation in the Punta de Mata ridge

This ridge is located in the central part of the study area (Fig. 5A). As with the other ridges, it is limited to the south by a strong scarp with a vertical offset of ~105 m. It is 25 km long and trends approximately NE-SW and it reaches 290 m high, decreasing to an average height of 130 m (Fig. 5C). In the field to the north of the Punta de Mata ridge ("4S" on Fig. 5A), an abnormal contact is observed between horizontal red and yellowish clays and siltstones at the bottom ("P1 and R1" on Fig. 6B), and at the top blueish clays, silts and pebbles ("N" on Fig. 6B) dipping ~25° to the SE. We interpreted this contact as a reverse fault. Above these bluish siltstones in the hanging-wall of the fault, the yellowish layer ("R" on Fig. 6B) could be the uplifted section of the yellowish basal unit observed in the foot-wall ("R1" on Fig. 6B) indicating a vertical offset of a few meters. The thickness of this yellow layer ("R" on Fig. 6B) decreases from 1.5 m to zero meters to the NW; i.e., toward the fault trace. Then, it shows layers thinning northward but with dip increasing downward in the section, suggesting growth strata geometry. Above this unit, another red layer similar ("P" on Fig. 6B) to the red one observed ("P1" on Fig. 6B) above the yellow one in the footwall also displays growth strata. These growth

strata indicate progressive uplift above the reverse fault. The outcrop is topped by alluvial deposits sampled for dating (sites 4S and 6S in Fig. 5A). For this site, the exposure age estimated from ^{10}Be and ^{26}Al method was ~14-15 ka.

4.2.3 Quaternary deformation in the Amarilis ridge

The Amarilis ridge is located in the south of the study area (Fig. 5A). The elevation of the ridge along the strike is approximately constant around 200 m, and it is truncated by the Amana River to the east. Its height decreases from 200 m at the north to 70 m to the south (Fig. 5D). The relief of the ridge is interpreted as flexure of the topographic surface, though we did not observe clear evidence of deformation. DEM shows that the Amarilis ridge marks the southern limit of the deformation front in the MFTB (Fig. 1). To date this folding, we took a sample from an alluvial terrace located in the northwest part of the Amarilis zone, on the left bank of the Amana River ("9S" on Fig. 5A). According to ^{10}Be and ^{26}Al results, the Amarilis ridge shows a burial time higher than ~1 Ma and an initial erosion rate between 10^{-4} and 5.10^{-6} m/y. The exposure age calculated by ^{10}Be and ^{26}Al method was ~25 ka (Table 1).

4.2.4 Quaternary deformation in the Jusepín ridge

The Jusepín ridge located to the east of the MFTB has a length of 28 km, an approximately E-W trend, and a mean elevation of 120 m (Fig. 5A). The elevation decreases eastward along the strike (Fig. 5E). The greater heights, around 180 m are located to the NW and decrease 50 m southwards approximately. An NW-SE topographic profile shows two slope-breaks, which were interpreted as fault scarps because they correspond to faults located in geological maps and to thrusts observed in seismic profiles (Fig. 5E). The across strike morphology of the ridge is also compatible with the asymmetric shape of a fault propagating fold; in particular, the northward slope of the backlimb allows discarding an erosional origin. This ridge is associated with the Jusepín thrust activity, which deviates strongly the drainage. Regionally, the upper reaches of the Guarapiche River flow across the SDI in N-S direction. Then, the lower reaches of the river flow in a NW-SE direction. Once again, in the Jusepín zone, the Guarapiche River drainage network changes its course abruptly to W-E direction parallel to the Jusepín ridge. The drainage pattern visible on the hanging-wall block is characterized by short and deep stream incisions along tributary creeks located at the foot of the scarp, and by long antecedent streams that cross-cut the whole structure (Fig. 5A). This indicates a morphological asymmetry typical of an active folding.

An asymmetric local drainage pattern developed around the Jusepín ridge suggests ongoing activity. Moreover, the natural trench in its middle part shows that yellow silts and clays are topped by alluvial deposits ("11" on Fig. 5A). These alluviums are folded (8 m of amplitude) and the relief here is a structural surface (Fig. 6C). A few hundred meters in front of that structure ("12S" on Fig. 5A); another fold is observed in alluvium with an amplitude ~5 meters, and asymmetry of folding that shows a north verging fold (Fig. 6D). ^{10}Be and ^{26}Al results show that the surface exposure history of the Jusepín ridge can only be explained by a burial time greater than ~1 Ma with an initial erosion rate between 10^{-4} and 10^{-5} m/y. The exposure age estimated for this site was ~35 ka (Table 1).

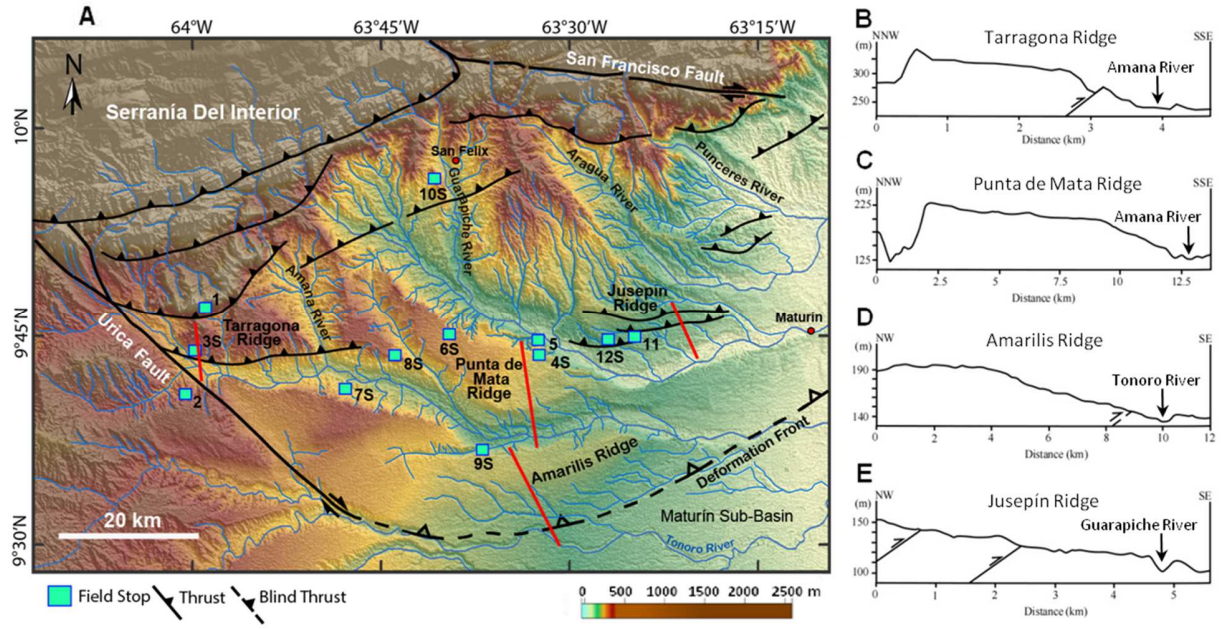

Fig.5. Superficial structures are showing evidence of recent deformation in the MFTB. A. Location map. Topographic profiles across ridges (B to E) represented by red lines.

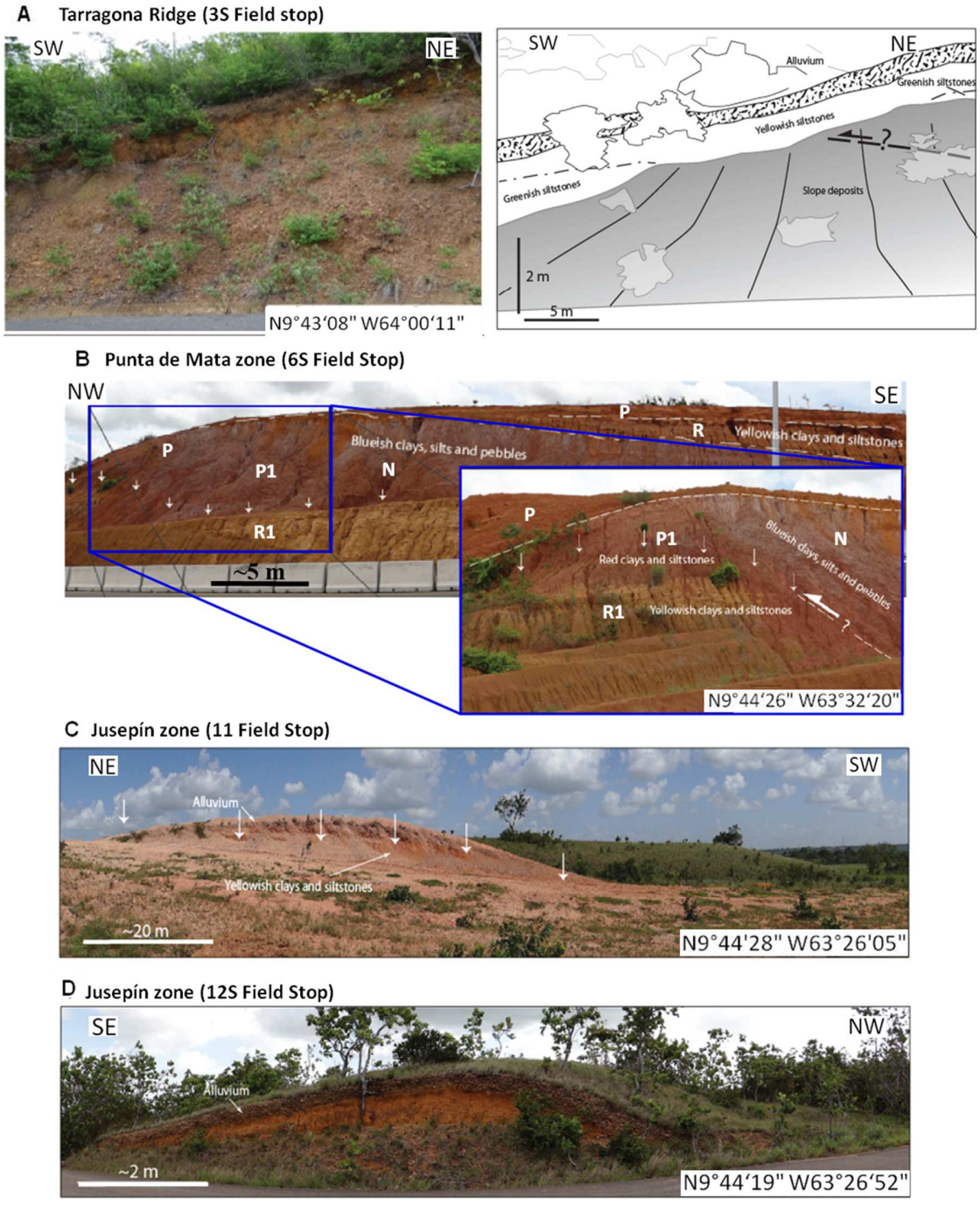

Fig. 6. Field stop pictures. A. Reverse faulting associated with the Tarragona thrust. B. T4S terrace in the Punta de Mata ridge, detail photo shows the possible reverse fault trace (arrows) that places the bluish clays, silts, and pebbles layer in contact with the red clays, siltstone, and yellowish clays basal layer. C. Tilted and folded terrace, white arrows point out the folded and tilted alluvium layer towards the SW. D. 12S terrace, note the tilting and folding of the alluvium layer. See Fig. 5A for location.

4.3 Vertical deformation rate from surfaces exposure

In the Tarragona, Punta de Mata, Amarilis, and Jusepín zones, we estimated a minimum vertical deformation of the terraces dated based on the exposure age obtained from ^{10}Be and ^{26}Al cosmogenic nuclides method, and on the vertical offset calculated in these terraces. The vertical deformation in the study area varies from 0.6±0.3 mm/y in the Amarilis zone to 0.1±0.1 mm/y in the Jusepín and Punta de Mata zones (Table 2).

Table 2. Surfaces exposure age from ^{10}Be and ^{26}Al cosmogenic nuclides and minimum vertical deformation rate calculated in the MFTB.

Site	Terrace	Latitude (N)	Longitude (W)	Elevation (m)	Estimated Age (ka)	Vertical offset (m)	Minimum vertical deformation rate (mm/y)
3S (Tarragona)	T3S	9°43'48"	64°00'07"	287	90 ± 5	30 ± 5	0.3 ± 0.3
4S (Punta de Mata)	T4S	9°44'14"	63°32'20"	204	15 ± 5	1.7 ± 1	0.1± 0.1
6S (Punta de Mata)	T6S	9°45'03"	63°39'23"	265	14 ± 5	----------	----------
9S (Amarilis)	T9S	9°36'42"	63°36'52"	175	25 ± 5	15 ± 2	0.6 ± 0.3
12S (Jusepín)	T12S	9°44'19"	63°26'52"	95	35 ± 5	3.5 ± 1	0.1± 0.1

4.4. Seismic interpretation

Based on stratigraphic markers from wells (e.g., Sánchez et al., 2010) and seismic data acquired by PDVSA in the MFTB, we interpreted four seismic horizons (Figs. 2 and 7A). From bottom to top: 1) top of Paleocene-Oligocene units (in the hanging wall and the foot-wall of the Furrial thrust), 2) Middle Miocene Unconformity (MMU), 3) Late Miocene Unconformity (LMU) and 4) one horizon in intra Plio-Pleistocene units (Mesa/Las Piedras Formation). The main faults interpreted were: the Pirital, Jusepín, Furrial, and Amarilis faults. We described each horizon and fault in the M1, M2, M3, M4, and M5 seismic lines (Figs. 7-9). The seismic lines are oriented N-S and are almost perpendicular to the superficial structures identified in the field, aerial photo, and, or DEM.

4.4.1 Seismic section analysis

M1 seismic line located to the east of the Urica fault shows a section to the south of the SDI characterized by a thrust belt (Fig. 7A). We identified three structures at different depths (Fig. 7B). The deepest structure is formed by two thrust sheets with south vergence and 30° north-dipping, exhibiting Cretaceous to Paleo-Oligocene rocks. The Tarragona thrust is located above these thrust sheets and involves pre-Cretaceous (Jurassic?) to Paleo-Oligocene rocks with a possible detachment in pre-Cretaceous rocks. The thrust sheet associated has an estimated thickness of ~7 km with southerly vergence and a 20° dip towards the north. On top of the Tarragona thrust sheet, there is an anticline named by us the Tarragona high developed in rocks of early-middle Miocene Carapita Formation (Fig. 2). The late Miocene and Plio-Pleistocene sequences onlap this shallow anticline, which reaches the surface through compression and uplifting generated by the Tarragona thrust.

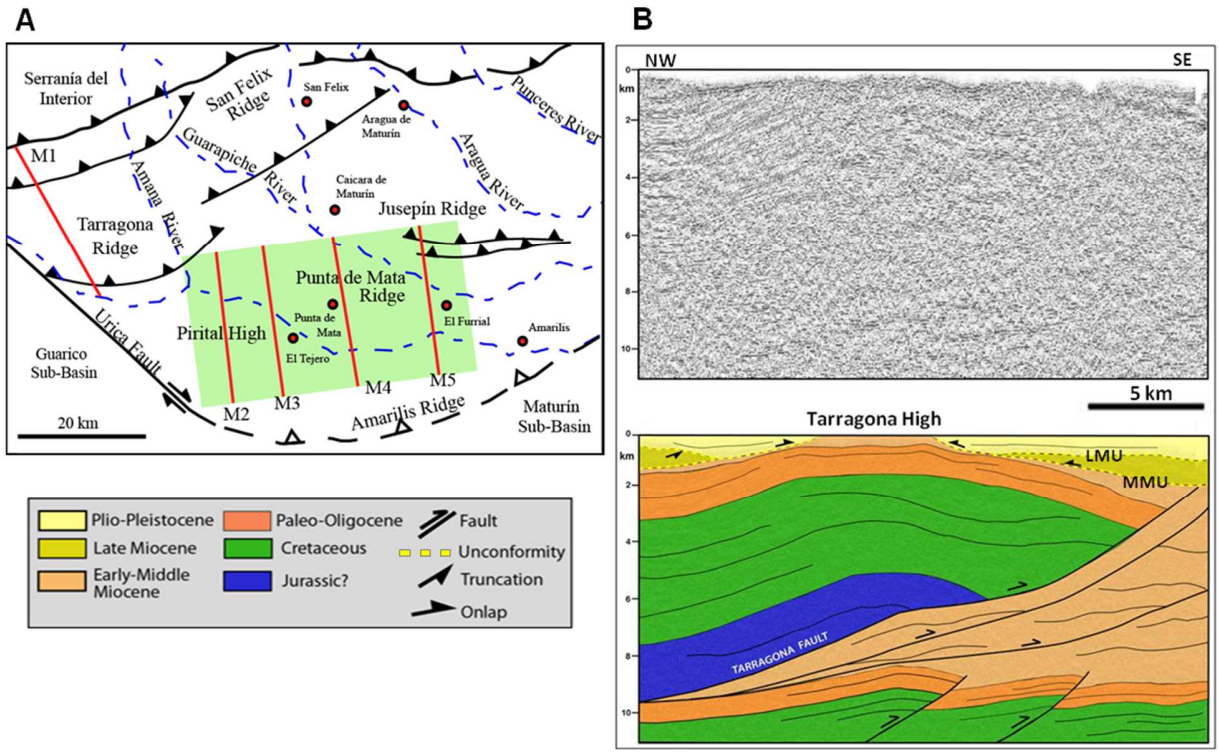

Fig. 7. A. Surface map of the study area showing seismic lines (red lines) and 3D seismic block (green square). B. M1 seismic line. Uninterpreted section (top), and interpreted section (bottom). LMU: Late Miocene Unconformity, MMU: Middle Miocene Unconformity.

M2 and M3 seismic lines are NNW-SSE sections of the 3D seismic located in the Punta de Mata ridge (Fig. 7A). Here, the Pirital and Furrial thrusts are observed (Figs. 8A and 8B). The Furrial thrust is located at the

bottom of the seismic line, shows 20° north-dipping strata in the hanging wall and a transport direction towards the south of ~ 4 km thick Cretaceous to Paleo-Oligocene units. Above the Furrial thrust is located the Pirital thrust that displays 15° north-dipping strata in the hanging wall and transports ~3.5 km of pre-Cretaceous to Paleo-Oligocene units towards the south. The thrust sheet associated with the Pirital thrust is in contact with early-middle Miocene units, which are also displaced and folded by this thrust, forming a shallow anticline named the Pirital high. The overlying layer composed of late Miocene unit changes in thickness on each side of this high. At the south flank, the La Pica Formation shows onlap termination towards the Pirital high, indicating that uplifting was active at the time of sedimentation (syn-tectonic deposits). At the north flank, the late Miocene unit is represented by the Morichito Formation, which filled a mini basin developed by the intense thrusting of the underlying structures (Figs. 2, 8A and 8B).

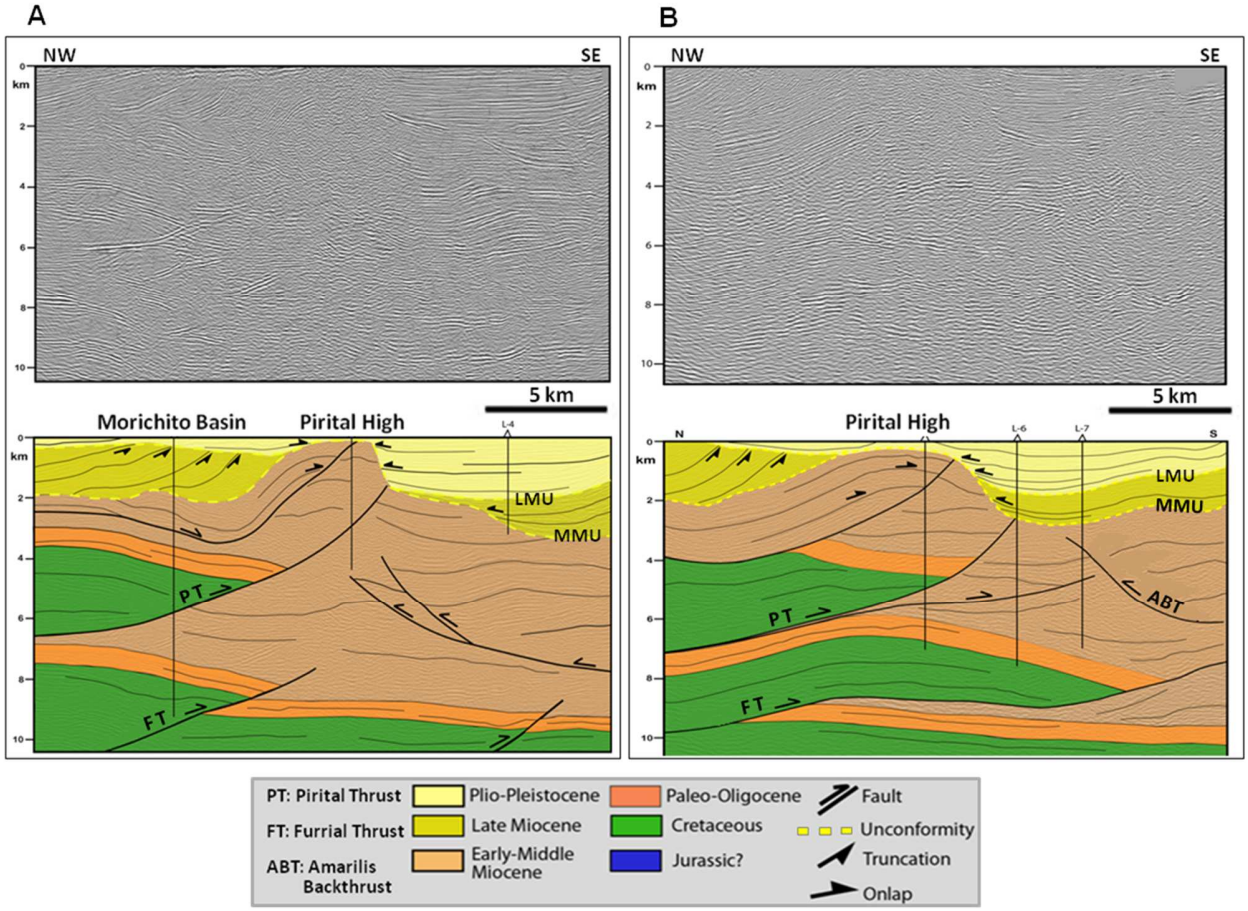

Fig. 8. A. M2 seismic line. B. M3 seismic line. Uninterpreted section (top), and interpreted section (bottom). LMU: Late Miocene Unconformity; MMU: Middle Miocene Unconformity; PT: Pirital Thrust; FT: Furrial Thrust; ABT: Amarilis Back Thrust. See Fig. 7A for location.

The late Miocene unit shows truncation toward in the top against the regional MMU, indicating active uplifting and an erosive episode developed in the northern part of the basin before the deposition of the Plio-Pleistocene units. Finally, the Pliocene-Pleistocene units onlap the emerging Pirital high evidencing that the active uplifting in the area exceeds the sedimentation rate. Also, these units are gently folded due to active thrusting in the deep structures. M3 seismic line shows the development toward the east of the Pirital high, Furrial, and Pirital thrusts (Fig. 8B). Here, the Furrial thrust increases its development towards the south, showing a possible detachment level in the Paleo-Oligocene units, and the Pirital thrust sheet is eroded coming into contact with the early-middle Miocene unit.

M4 seismic line shows the advance of the Furrial thrust towards the south and how the Pirital high begins to disappear in this same direction (Fig. 9A). The Furrial thrust exhibits similar geometry as observed in the M3 seismic line, the fault cut-off is in the same location through the entire 3D seismic block. In the M5 line, the Amarilis backthrust dips 35° to the south, and its associated thrust sheet is a ~3.6 km thick section of the early-middle Miocene Carapita Formation (Fig. 9B). The late Miocene to Plio-Pleistocene units above the Amarilis backthrust display growth strata geometry. Also, these units were folded, creating the Amarilis high, which is the shallower structure in this profile.

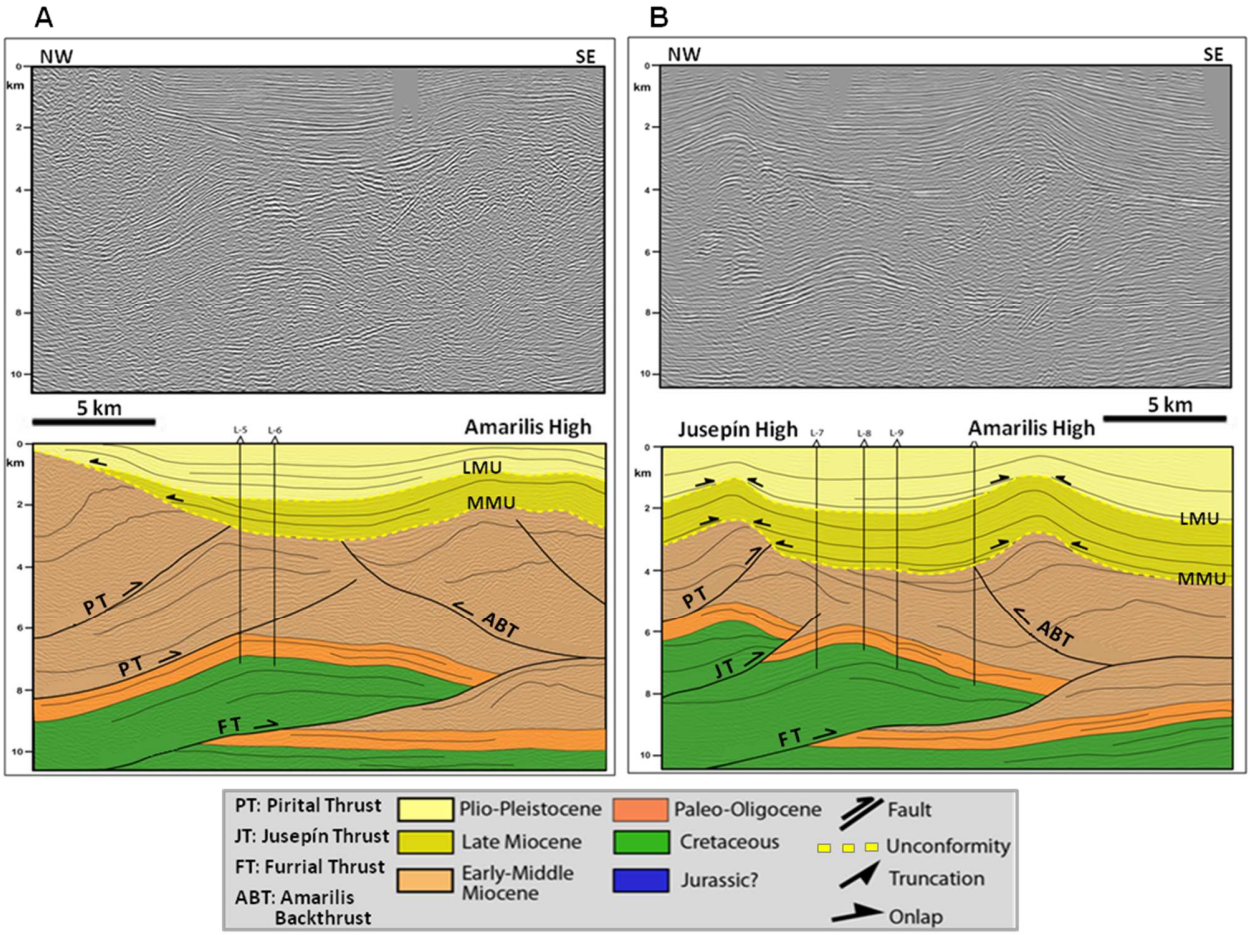

Fig. 9. A. M4 seismic line. B. M5 seismic line. Uninterpreted section (top), and interpreted section (bottom). LMU: Late Miocene Unconformity, MMU: Middle Miocene Unconformity, PT: Pirital Thrust, FT: Furrial Thrust, ABT: Amarilis Back Thrust, JT: Jusepín Thrust. See Fig. 7A for location.

4.4.2 Structural and Isochron depth maps

The maps were extracted from seismic interpretation carried out on the entire 980 km^2 of 3D depth migrated seismic data, including the M2 to M5 seismic lines shown in the previous section. The LMU structural depth map shows the structural trend of the Pirital, Amarilis y Jusepín highs (Fig. 10A). In this level, the Pirital high extends from the west to the north part of the seismic block. To the west, its strike is N65E and to the north N35E. The Pirital high top is located between -600 and -1000 m depth (see the north-central part in Fig. 10A). The Morichito basin dips towards the north, reaching a depth of ~ -2000 m. The Jusepín high is located to the northeast at ~ -800 m depth, and the Amarilis high to the south at ~ -400 m depth, both highs have N70^{o}E structural trend. Moreover, the Pirital high exhibits the same orientation in the MMU and LMU structural

maps; however, in the MMU map, this is eroded toward the northeast (Fig. 10B), indicating that the uplifting has been occurring in different episodes since the development of the Pirital high. The Jusepín high is not clearly defined in this map; whereas, the Amarilis high reaches its top at ~ -2000 m depth. In the northwest, the Morichito basin reaches its maximum depth of ~ -3500 m (Fig. 10B).

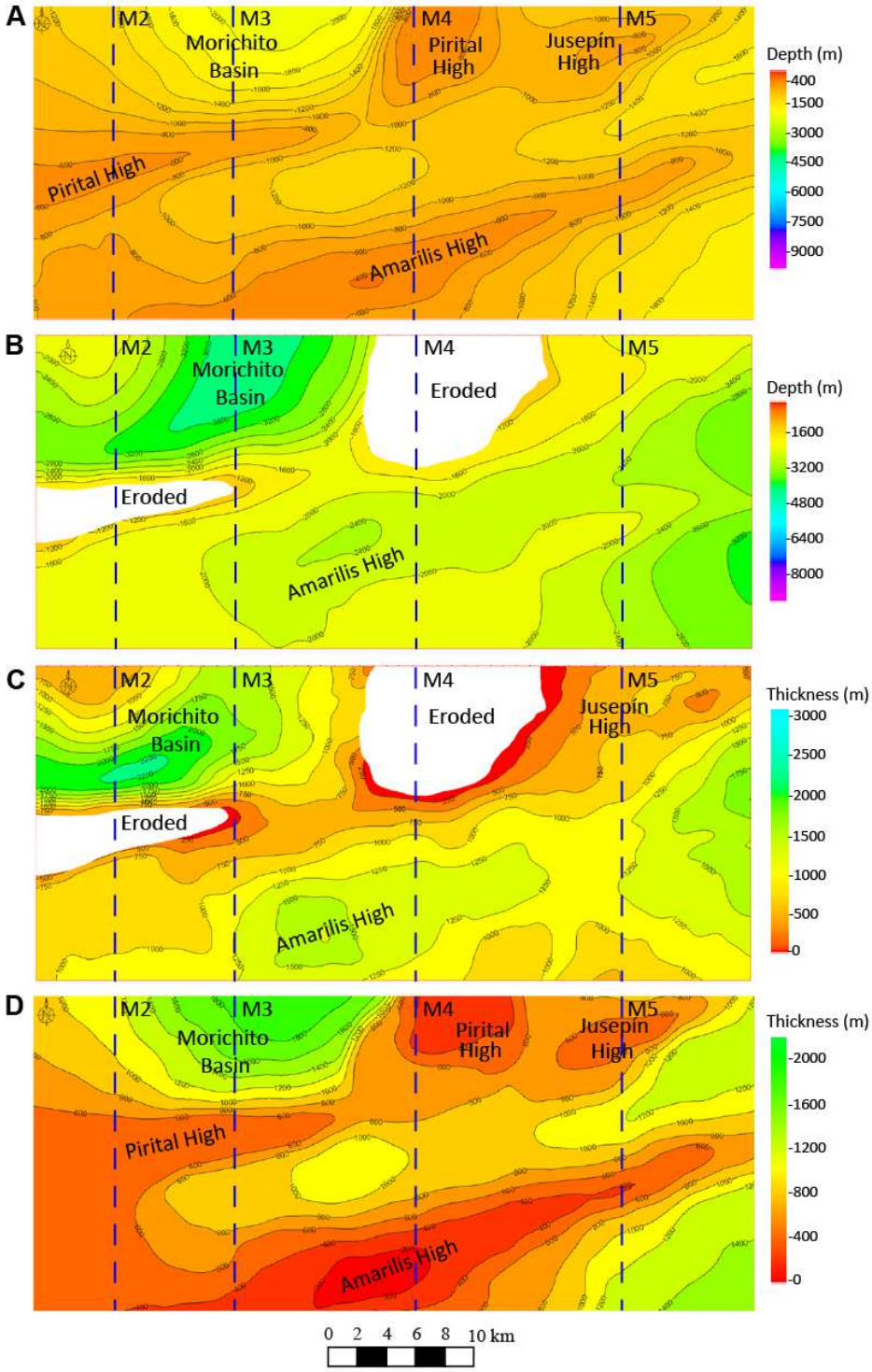

Fig. 10. Structural and isochron depth maps obtained from 3D seismic data depth migrated. A. Late Miocene Unconformity (LMU) B. Middle Miocene Unconformity (MMU) C. Isochron depth map from MMU to LMU D. Isochron depth map from LMU to Plio-Pleistocene top.

The post-MMU units display growth strata geometry, and hence, their thicknesses are controlled by the active tectonic in the area. This is shown on the isochron maps that display MMU-LMU and LMU-Plio-Pleistocene thicknesses variations (Fig. 10). The MMU-LMU isochron map shows the Pirital high top eroded and thicknesses increasing away from the high (Fig. 10C). At the northeast part, thickness increases towards the east with values from 0 to 1000 m, while to the southwest, thickness increases away from the high from 0 m to 600 m. The same is observed in the western part of the Pirital high; here, thicknesses increase more rapidly to the north where the main tectonic loading is taking place. The same behavior is observed for the Pirital high in the LMU-Plio-Pleistocene isochron map, with a general increasing of thicknesses to the NNW and SSE away from the high. To the south, thicknesses increase around and away the Amarilis high is less strong (Fig. 10C), showing that this high formed after the LMU, this is shown in the LMU-Plio-Pleistocene isochron map that displays thicknesses increasing away from the Amarilis high from 0 to 1000 m (Fig. 10D). The thicknesses variations around the Jusepín high is as the Amarilis high, little changes between the middle and late Miocene (Fig. 10C) and higher thicknesses changes in LMU-Plio-Pleistocene interval were thicknesses change from 300 to 600 m away from the high (Fig. 10D).

4.4.3 Uplift rate from seismic lines

Along the M1 seismic line, the LMU is folded and eroded to the north (Fig. 7B). Assuming the geometry of the eroded part, we estimated a vertical offset of ~1.5 km, and calculated an uplift rate of ~0.3 mm/y. Along the M2 and M3 seismic lines, the LMU horizon is deeper to the south than to the north, and the offset observed is related to the Pirital thrust (Figs. 8A and 8B). Based on this, for the M2 we estimated a vertical offset of 1.9 km, and calculated an uplift rate of ~0.4 mm/y, and for the M3 a vertical offset of 1.7 km that yield an uplift rate of ~0.3 mm/y. Along the M4 line, the LMU was folded and partly eroded to the north of the cross-section (Fig. 9A), here we measured a vertical offset of ~1.6 km, which yield an uplift rate of 0.3 mm/y. Along the M5 line, we estimated a vertical offset of ~1.5 km, yielding an uplift rate of ~0.3 mm/y (Table 3).

Table 3. Uplift rate and shortening of the Plio-Pleistocene units calculated from seismic lines.

Seismic line	Seismic line length (km)	LMU vertical offset (km)	Uplift rate (mm/y)	Shortening (km)	Shortening (%)
M1	22	1.5	0.3	1.3	6
M2	20	1.9	0.4	1.0	5
M3	20	1.7	0.3	1.0	5
M4	20	1.6	0.3	0.7	4
M5	20	1.5	0.3	0.5	3

4.4.4 Shortening quantification from seismic lines

The LMU is the base of the Plio-Pleistocene units (Fig. 2), for this reason, we calculated the N-S shortening using this unconformity as a key horizon, from west to east we obtained a minimum shortening of ~1.3 km along the M1 seismic line, ~1 km for the M2 and M3 seismic lines, ~0.7 km along the M4 seismic line, and ~0.5 km on the M5 seismic line (Figs. 6-8). The shortening is more significant to the west, near the Urica fault reaching 6% (M1 seismic line), and it decreases toward the east (M5 seismic line) up to 3% (Table 3).

5. Discussion

5.1 Neotectonics in the MFTB from surface analysis

The analysis of the terrace ages obtained by the ^{10}Be and ^{26}Al method describes a complex evolution. Indeed, it suggests that the rocks sampled on the terraces had a possible inherited cosmogenic nuclides concentration before being placed and stored within the terrace. The rocks were probably transported from the Cretaceous units exposed in the SDI until being deposited in the foothills and the foredeep of the Maturín Sub-basin. During the Plio-Pleistocene the samples were buried, stored, and finally re-exhumed during the terrace formation. According to the ^{10}Be and ^{26}Al dating results, all the terraces were exposed during the late Pleistocene (the oldest 90 ka at the 3S site and the most recent 15 ka at the 4S site) (Table 2). Additionally these river terraces showed one or more deformation markers such as steep slopes, tilting, folded surfaces, and faulting; indicating that tectonism in the area was active even after terraces were exposed to the surface. The Urica fault activity is affecting the vertical deformation rate variation in the MFTB (Table 2). The highest rates occur in the Tarragona (0.3 ± 0.3 mm/y) and Amarilis ridges (0.6 ± 0.3 mm/y) both of them near the Urica

fault, decreasing to the east as it becomes more distant from the Urica fault as the Punta de Mata and Jusepín ridges (0.1±0.1 mm/y).

Similarly, comparing the heights of the ridges we observe that the Tarragona ridge situated to the NW closer to the SDI is higher than the Amarilis and Jusepín ridges located to the SE (Fig. 5A). These differences in height suggest that the tectonic activity has been greatest and, or has lasted longer to the NNW than to SSE of the MFTB.

5.2 Growth strata pattern in the MFTB

Growth strata are the units deposited during deformation around a growing fold. It provides information on kinematics, timing, and mechanisms of folding according to the patterns of strain shown above fold limbs (Suppe, 1992; Poblet et al., 1997; McClay, 2004; Shaw and Hook, 2005). Folded unconformities and growth strata geometries indicate that in the MFTB, several episodes of compression and exposition took place, which also controlled the sediment deposition expressed in growth strata geometry (Fig. 11). Also, the isochron depth maps of the post-MMU units evidence substantial variations in the sediment thickness from west to east (Figs. 10C and 10D).

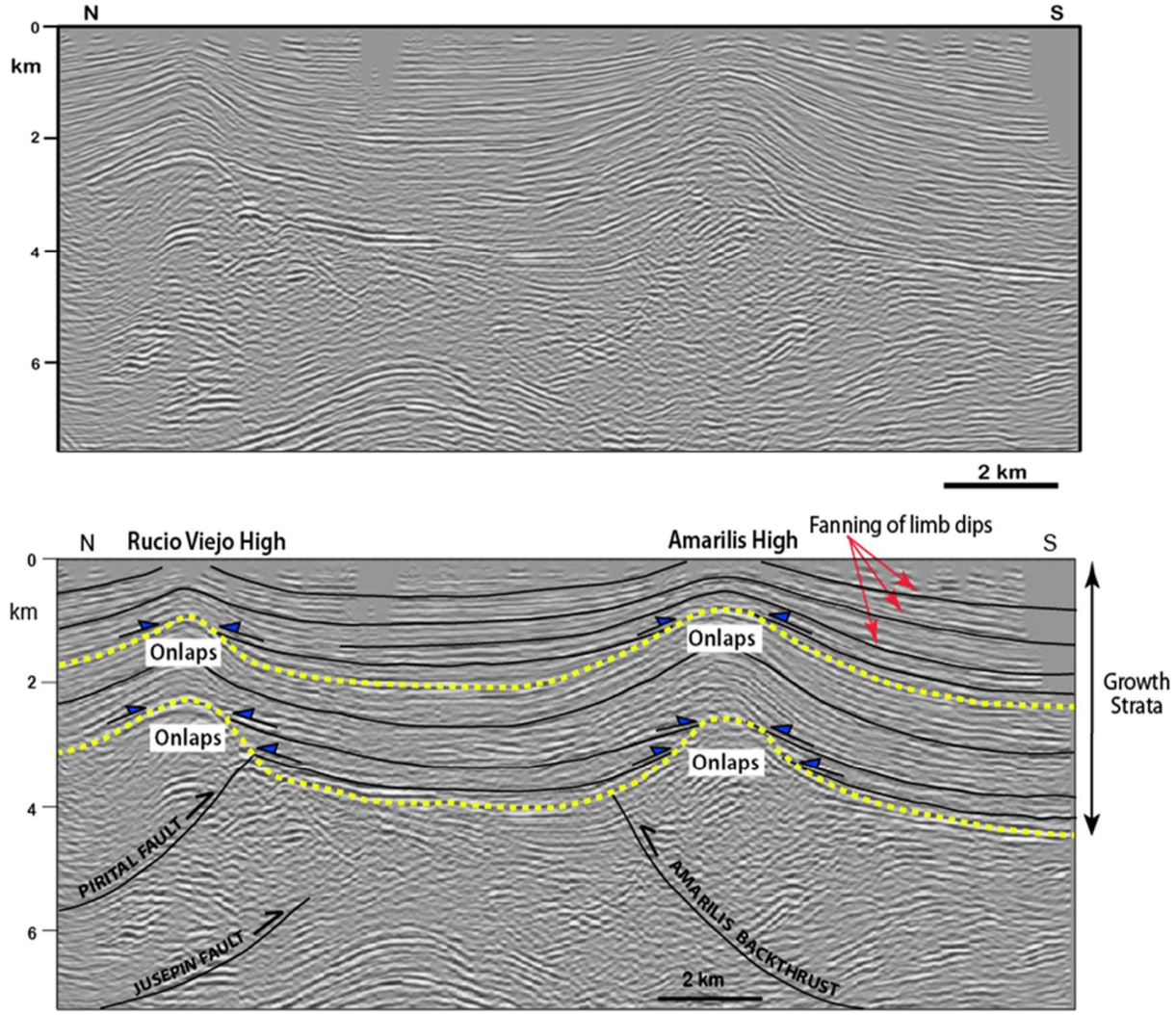

Fig. 11. Detail of M5 seismic line showing the growth strata configuration in the MFTB. See Fig. 7A for location.

5.3 Neotectonics in the MFTB from the relation between deep and surface structures

The Tarragona high located to the northwest of the study area in the foothill of the SDI is an anticline formed by early-middle Miocene shale units. The seismic section on this high shows that sedimentary deposits from the late Miocene to the Plio-Pleistocene are folded and they form growth strata geometry at its flanks (Fig. 7B). The dips of these strata are steeper in the oldest growth strata, showing a progressive fanning of the limbs dip, being this geometry the main characteristic of the limb rotation mechanism in contractional fault-related folds (Poblet et al., 1997; Shaw and Hook, 2005). Additionally, these growth strata onlap the Pirital and Tarragona highs to the north and onlap the Amarilis and Jusepín highs to the southeast, evidence that the compression was active at the time of the sedimentation, and that the uplift rate exceeded the sedimentation

rate (Figs. 7-9). The southward propagation of the Tarragona thrust deformed the pre-Cretaceous to Paleo-Oligocene units with detachment level in pre-Cretaceous units, later this thrust was reactivated as an out-of-sequence structure that uplifted the shale units (Carapita Formation) and generated the Tarragona high (Fig. 7B). Surface expression of the Tarragona high is observed in DEM imagery as a ~350 m high ridge oriented in N80E direction named by us Tarragona Ridge (Figs. 12). At the 3S site is an outcrop of early-middle Miocene shales, where active deformation related to the Tarragona thrust places in contact yellowish and greenish shales and folds an alluvium layer at the top of the outcrop (Fig. 6A).

As with the Tarragona, the Pirital thrust was reactivated during an out-of-sequence event, uplifting and deforming the overlying shale unit and formed the Pirital high (Fig. 7). The structural depth map of the MMU shows that the Pirital thrust strongly affected the post-middle Miocene units (Fig. 10B). In the Punta de Mata zone, at the 4S site (Fig. 5A) we describe an outcrop ~5 m high and ~25 m long located above the northeast termination of the Pirital high and faulted by a backthrust dipping to the south. This ridge is a surface expression of the Pirital high, indicating that the compressive system is still active (Fig. 12).

Additionally, the late Miocene to Plio-Pleistocene units show onlap termination on both sides of the Pirital high; this onlap termination defines growth strata geometry (Fig. 8). We also observe this growth strata geometry in the 4S site, where yellowish clays and siltstones show onlapping geometry (Fig. 7B). The presence of the growth strata geometry in depth and surface, the folded late Miocene to Plio-Pleistocene units, and the ridges observed in the field are evidence of the active deformation in the MFTB, but less intense than in the Tarragona zone (Fig.12).

The Jusepín ridge also displays correspondence between surface deformation and subsurface features, (Fig. 12) as reported by Wagner (2004) in other areas located further north. In the subsurface, the Pirital thrust is a fault dipping 30° north that displaces and deforms early-middle Miocene shales. This displacement generated growth strata geometry, uplifting, and gently folding of the late Miocene to Plio-Pleistocene units, creating the Jusepín high (Fig. 9B). On the surface, from DEM and aerial photos, several south vergence thrusts were identified just above the Jusepín high (Figs. 5A and 5E). These thrusts tilt and deform the alluvial terraces observed in sites 11 and 12S (Figs. 5A, 6C, and 6D).

The Amarilis ridge is the southernmost surface expression of the deformation due to the underlying thrust system (Fig. 12). The ridge is related vertically to the Amarilis high, is 19 km long and 6.5 km wide, and reaches 200 m in height (Fig. 12). In the subsurface, the north verging Amarilis backthrust is located to the

south of the MFTB and is associated with the southern limit of the Furrial thrust (Fig. 13). The thrust sheet of the Amarilis backthrust is composed of early Miocene units with a thickness of 3.6 km and similarly as in the Jusepín high, the late Miocene to Plio-Pleistocene deposits have growth strata geometry product of the active uplifting (Fig. 9B).

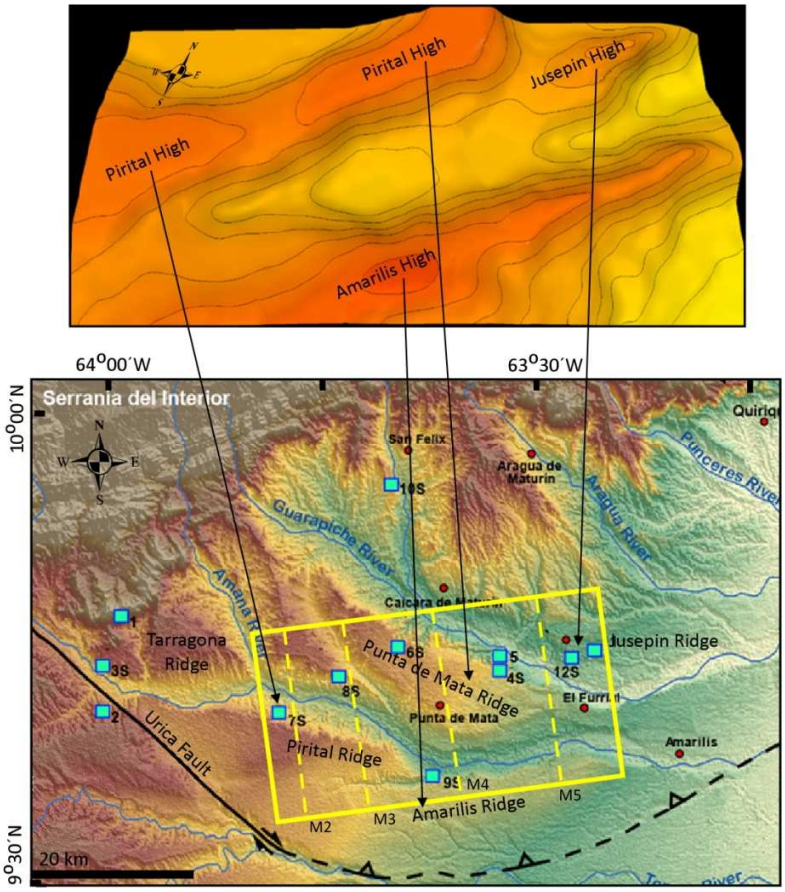

Fig.12. Relation between deep and surface structures. Pleistocene structural map in depth showing subsurface highs (above). DEM showing the ridges (below).

5.4 Uplift rate and shortening in the Plio-Pleistocene units

To the west, the shortening is mainly caused by the Tarragona thrust, in the center part by Pirital thrust and to the south, by Furrial thrust and Amarilis backthrust (Fig. 13). Seismic lines show that the post-middle Miocene

units are more deformed to the west of the MFTB near the Urica Fault, where the large Tarragona and Pirital thrusts are better developed (Figs. 7B and 8A). The same is observed at the surface, where deformation progressively decreases towards the east; for example, the surface expression of the Pirital high in the Punta de Mata zone, named by us Punta de Mata ridge slowly decreases to the east until it disappears (Fig. 12). More to the east, seismic data shows that folds and shortening in the Plio-Pleistocene units are smaller compared to western area.

The comparison between the MMU and LMU depth maps show that the post-middle Miocene deformation in the MFTB occurred differently in the NW and SE parts of the area (Figs. 10A and 10B). To the NW, the M1 seismic line shows that the MMU truncates the units below; this unconformity was slightly folded and tilted before the Tarragona thrust activity formed the LMU. Then, a new deformation event took place creating the LMU which also truncates the late Miocene unit. Toward the east, in the M2 and M3 seismic lines the geometry of the MMU and LMU unconformities reflects the middle Miocene Pirital out-of-sequence thrusting (Figs. 8A and 8B). This event formed the Pirital high and produced the difference in thickness between the post-Middle Miocene deposits to the north and south of the high.

From seismic interpretation, we estimated an average Plio-Pleistocene uplift rate on the order of 0.3 mm/y for the last 5.3 Ma (Table 3). This rate is comparable to the vertical deformation rate calculated in this work, using the vertical offset in the surfaces exposure and the age calculated with cosmogenic nuclides (Table 2) where the greatest rates are occurring to the NNW near the Urica fault in the Tarragona ridge (0.3±0.3 mm/y) and the Amarilis ridge (0.6±0.3 mm/y) but these decrease to the SSE away from the Urica fault in the Jusepín and Punta de Mata ridges (0.1±0.1 mm/y). Similarly, the shortening is higher to the west (6%) and to the east away from the Urica Fault (3%), showing that the post-LMU deformation is strongly controlled by Urica Fault activity (Fig. 13).

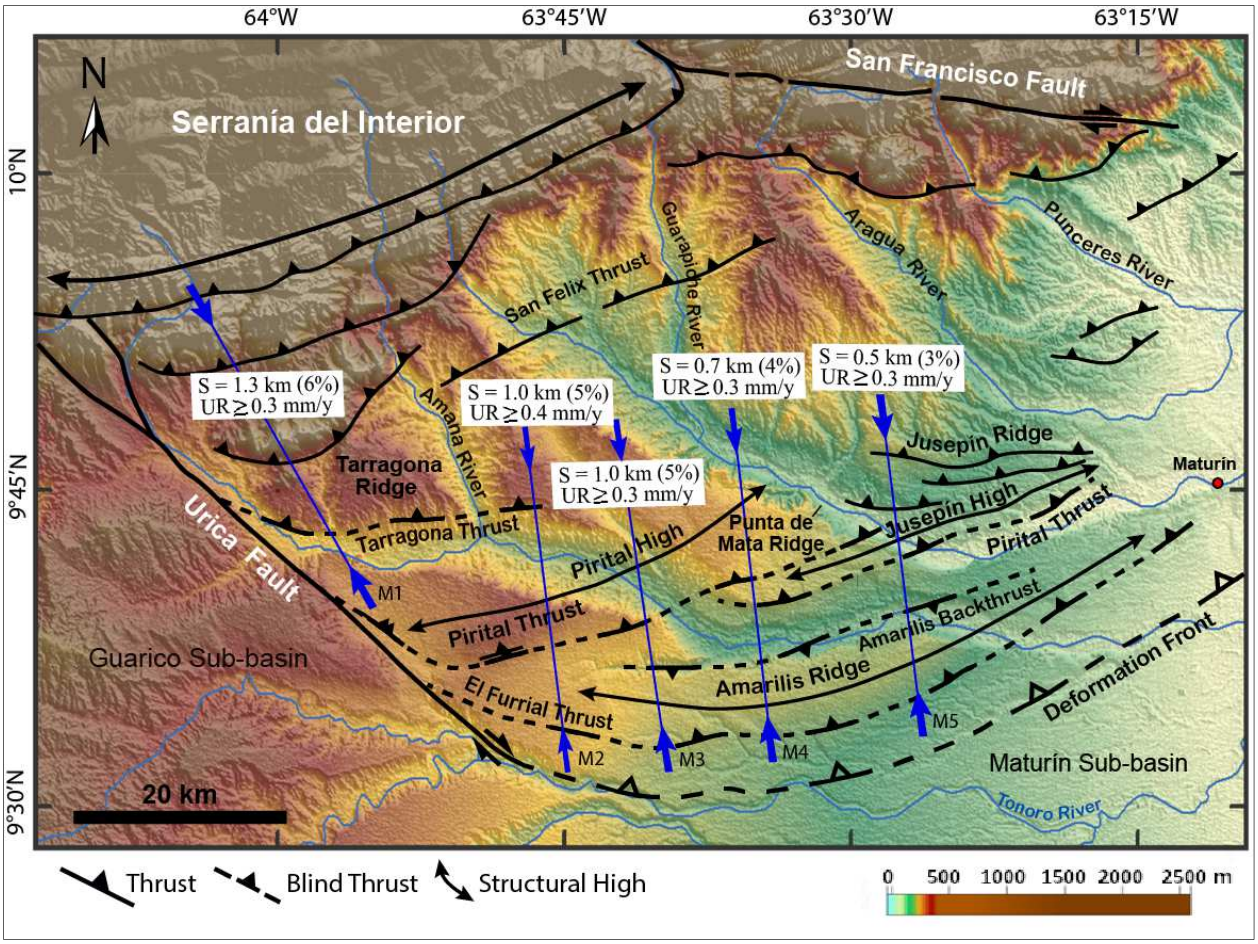

Fig.13.Tectonic map of the MFTB showing structural features interpreted from seismic lines, fieldwork, DEM and aerial photos. S: Shortening, UR: Uplift rate. Blue arrows indicate shortening direction calculated in the Plio-Pleistocene units.

6. Conclusions

Growth strata around structural highs, as well as folding and erosion of the Middle Miocene Unconformity (MMU) and the Late Miocene Unconformity (LMU), indicate that in the Monagas Fold and Thrust Belt (MFTB) several episodes of compression and exposition took place since the middle Miocene. The terrace ages estimated by the ^{10}Be and ^{26}Al methods show that these were exposed during the late Pleistocene, being the oldest of 90±5 ka and located in Tarragona ridge and the youngest being of 15±5 ka and located in the Punta de Mata ridge. Field evidence of folded, tilted and faulted terraces demonstrated that the tectonics in the area was active even after they were exposed to the surface.

The highest uplift rates calculated from cosmogenic nuclides data are located to the NNW near the Urica fault: 0.3±0.3 mm/y for the Tarragona ridge, and 0.6±0.3 mm/y for the Amarilis ridge. The rates decrease to the SSE away from the Urica fault: 0.1±0.1 mm/y for the Jusepín and Punta de Mata ridges. Similarly, the post-LMU shortening ratio drops from NNW (6%) to SSE (3%). Surface observations corroborate that the heights of the ridges decrease towards the SSE.

Based on these geomorphological, geochronological and seismic results, we propose that since 10 Ma (post-middle Miocene), the Serranía Del Interior (SDI) is being affected by a clockwise rotation of 3.7º Ma^{-1} related to the development of a synthetic Riedel shear system formed by the El Pilar fault as the master regional fault and by the Urica and San Francisco faults as synthetic Riedel shears (Fajardo, 2015). Part of this movement is being transferred southwards in the MFTB as a local compressive deformation through the horsetail splays interpreted that marking the southern termination of the Urica fault. As a consequence, older thrusts, such as the Tarragona and Pirital thrusts, were reactivated out-of-sequence. The propagation of these thrusts towards the south and the secondary thrust development have uplifted the post-middle Miocene units until they reach the surface, creating the ridges, and deforming the river terraces in the area. Additionally, the horsetail termination causes the shortening to be more significant near the Urica strike-slip fault and smaller as it becomes more distant from the fault.

7. Acknowledgments

This work forms part of Atiria Fajardo's Ph.D. research at the Université de Pau et des Pays de l'Adour France. Atiria Fajardo wants to thank Fundación Gran Mariscal de Ayacucho (FUNDAYACUCHO); French Embassy

in Venezuela, Université of Pau et des Pays de l'Adour and Petróleos de Venezuela, S.A. (PDVSA) by supported me during my studies. The authors would like to thank Damien Dhont, who participated in the initiation of the project, Yves Hervouet and Jean-Paul Xavier, for supporting its development. We are also grateful to Dr. Frances McCarty, to the reviewers and editors who improved this paper with their comments and suggestions.

8. References

Algar, S. and Pindell, J. (1993). Structure and deformation history of the northern range of Trinidad and adjacent areas. Tectonics, 12, 814-829.

Audemard, F.A. (2000). Map of Quaternary Faults of Venezuela (1:2000000): United States Geological Survey, Venezuelan Foundation for Seismological Research. Instituto Tecnológico Venezolano del Petróleo S.A (INTEVEP), Petróleos de Venezuela S.A (PDVSA).

Audemard, F. A. (2006). Surface rupture of the Cariaco July 09, 1997 earthquake on the El Pilar Fault, Northeastern Venezuela. Tectonophysics, 424(1–2), 19–39, doi:10.1016/j.tecto.2006.04.018.

Audemard, F. A. (2011). Multiple-trench investigations across the newly ruptured segment of the El Pilar Fault in Northeastern Venezuela after the 1997 Cariaco earthquake. Geol. Soc. Am. Spec. Pap., 479, 133-157, doi:10.1130/2011.2479 (06).

Audemard, F., Romero, G., Rendon, H., and Cano, V. (2005). Quaternary fault kinematics and stress tensors along the southern Caribbean from fault-slip data and focal mechanism solutions. Earth-Science Reviews 69, 181–233.

Audemard, F. A., Singer, A., and Soulas, J. P., (2006). FUNVISIS Neotectonics Section, Quaternary faults and stress regime of Venezuela. Revista de la Asociación Geológica Argentina, 61, 480-461.

Avé Lallemant, H. G. (1997). Transpression, displacement partitioning, and exhumation in the eastern Caribbean/South American plate boundary zone. Tectonics, 16(2), 272-289.

Babb, S., and Mann, P. (1999). Structural and sedimentary development of a Neogene transpressional plate boundary between the Caribbean and South America plates in Trinidad and the Gulf of Paria. Sedimentary Basins of the World, 4, 495-557.

Beltrán, C., A. Singer, and J. A. Rodríguez (1996), The El Pilar Fault active trace (northeastern Venezuela): Neotectonic evidences and paleoseismic data, in Proceedings, 3rd International Symposium on Andean Geodynamics, pp. 153–156, Saint-Malo, France.

Desilets, D., Zreda, M., Almasi, P. F., and Elmore, D. (2006). Determination of cosmogenic ^{36}Cl in rocks by isotope dilution: innovations, validation and error propagation. Chemical Geology, 233(3), 185-195.

Di Croce, J., Bally, A.W., and Vail, P., (1999). Sequence stratigraphy of the Eastern Venezuelan Basin. In: Mann, P. (Ed.), Caribbean Basins. Sedimentary Basins of the World, v. 4. Elsevier Science B.V, Amsterdam, The Netherlands, pp. 419–476.

Duerto, L. (2007). Shale tectonics Eastern Venezuelan basin (Doctoral dissertation, Royal Holloway, University of London).

Dunai, T. J. (2001). Influence of secular variation of the geomagnetic field on production rates of in situ produced cosmogenic nuclides. Earth and Planetary Science Letters, 193(1), 197-212.

Fajardo, A. (2015). Neotectonic evolution of the Serranía Del Interior Range and Monagas Fold and Thrust belt, Eastern Venezuela: morphotectonics, seismic profiles analyses and paleomagnetism. Ph.D. dissertation, University of Pau, France.

FUNVISIS, 2020. Seismological activity. http://www.funvisis.gob.ve

González, C, J. et al., (1980). Geología de Venezuela y de sus cuencas petrolíferas. Ed. Foninves, vol. 2.

Jácome, M. I., Kusznir, N., Audemard, F., and Flint, S. (2003). Formation of the Maturín Foreland Basin, Eastern Venezuela: Thrust sheet loading or subduction dynamic topography. Tectonics, 22(5).

Jouanne, F., Audemard, F. A., Beck, C., Van Welden, A., Ollarves, R., and Reinoza, C. (2011). Present-day deformation along the El Pilar fault in Eastern Venezuela: Evidence of creep along a major transform boundary. Journal of Geodynamics, 51(5), 398-410.

Klein, J., Giegengack, R., Middleton, R., Sharma, P., Underwood, J. R., and Weeks, R. A. (1986). Revealing histories of exposure using in situ produced ^{26}Al and ^{10}Be in Libyan desert glass. Radiocarbon, 28(2A), 547-555.

Lal, D. (1991). Cosmic ray labeling of erosion surfaces: in situ nuclide production rates and erosion models. Earth and Planetary Science Letters, 104(2), 424-439.

L.E.V. (Léxico Estratigráfico Electrónico de Venezuela). (2011). http://www.pdv.com/lexico.

Lifton, N. A., Bieber, J. W., Clem, J. M., Duldig, M. L., Evenson, P., Humble, J. E., and Pyle, R. (2005). Addressing solar modulation and long-term uncertainties in scaling secondary cosmic rays for in situ cosmogenic nuclide applications. Earth and Planetary Science Letters, 239(1), 140-161.

Lingrey, S. (2007). Plate tectonic setting and cenozoic deformation of Trinidad: fold belt restoration in a region of significant strike-slip. In Thrust Belts and Foreland Basins. Springer Berlin Heidelberg, 163-178.

Mann, P., Schubert, C., and Burke, K. (1990). Review of Caribbean neotectonics. In: Geological Society of America (Ed.). The Geology of North America, vol. H. The Caribbean Region, Boulder, CO., 307-338.

Márquez, C., Benkovics, L., De Mena, J., Reveron, J., and Helwig, J. (2003). Seismic Structural Interpretation of the Northern Monagas Giant Producing Trend, Venezuela: Time versus Depth. In AAPG Annual Meeting 2003.

Meschede, M., and Frisch, W. (1998). A plate-tectonic model for the Mesozoic and Early Cenozoic history of the Caribbean plate. Tectonophysics, 296(3), 269-291.

McClay, K. R. (Ed.). (2004). Thrust Tectonics and Hydrocarbon Systems: AAPG Memoir 82 (No. 82). AAPG.

Nishiizumi, K., Lal, D., Klein, J., Middleton, R., and Arnold, J. R. (1986). Production of ^{10}Be and ^{26}Al by cosmic rays in terrestrial quartz in situ and implications for erosion rates. Nature, 319, 134-136.

Parnaud, F., Gou, Y., Pascual, J.-C., Truskowski, I., Gallango, O., Passalacqua, H. and Roure, F. (1995), Petroleum geology of the central part of the Eastern Venezuela Basin, in A. J. Tankard, R. Suárez S. and H. J. Welsink, Petroleum basins of South America: AAPG Memoir 62, 741–756.

Parra, M., Sánchez, G. J., Montilla, L., Guzmán, O. J., Namson, J., and Jácome, M. I. (2010). The Monagas Fold–Thrust Belt of Eastern Venezuela. Part I: Structural and thermal modeling. Marine and Petroleum Geology, 28(1), 40-69.

Pérez, O. J., Bilham, R., Bendick, R., Velandia, J. R., Hernández, N., Moncayo, C., and Kozuch, M. (2001). Velocity field across the southern Caribbean Plate boundary and estimates of Caribbean/South-American Plate movement using GPS geodesy 1994-2000 (Paper 2001GL013183). Geophysical Research Letters, 28(15), 2987-2990.

Pindell, J. L., and Barrett, S. F. (1990). Geological evolution of the Caribbean region: a plate tectonic perspective, in Dengo, G. and Case, J. E. (eds.), The Geology of North America, The Caribbean Region, Geological Society of America, V.(H), 405-432.

Pindell J., Higgs, R., and Dewey J. (1998). Cenozoic palinspastic reconstruction,paleogeographic evolution and hydrocarbon setting of the northern margin of South America. SEPM Special Publication, 58, 45-85.

Pindell, J. L., Kennan, L., Wright, D., and Erikson, J. (2009). Clastic domains of sandstones in central/eastern Venezuela, Trinidad, and Barbados: heavy mineral and tectonic constraints on provenance and paleogeography, in: James, K. H., Lorente, M. A. and Pindell, J. L. (eds) The Origin and Evolution of the Caribbean plate. Geological Society, London, Special Publications, 328, 743–797.

Poblet, J., McClay, K., Storti, F., and Muñoz, J. A. (1997). Geometries of syntectonic sediments associated with single-layer detachment folds. Journal of Structural Geology, 19(3), 369-381.

Reinoza, C., Jouanne, F., Audemard, F. A., Schmitz, M., and Beck, C. (2015). Geodetic exploration of strain along the El Pilar fault in Northeastern Venezuela. Journal of Geophysical Research: Solid Earth, 120(3), 1993-2013.

Roure, F., Bordas-Lefloch, N., Toro, J., Aubourg, C., Guilhaumou, N., Hernandez, E., Lecornec-Lance, S., Rivero, C., Robion, P., and Sassi, W. (2003). Reservoir Appraisal in the Sub-Andean Basins (Eastern Venezuela and Eastern Colombian Foothills). In: RTB in C. Bartolini and J. Blickwede eds., The Circum-Gulf of Mexico and the Caribbean: Hydrocarbon habitats, basin formation, and Plate tectonics. American Association of Petroleum Geologists, 750-775.

Sánchez, G., Baptista N., Parra, M., Montilla L., Guzmán O., and Finno A. (2010). The Monagas Fold–Thrust belt of Eastern Venezuela. Part II: Structural and palaeo-geographic controls on the turbidite reservoir potential of the middle Miocene foreland sequence. Marine and Petroleum Geology. DOI:10.1016/j.marpetgeo.2010.01.021.

Shaw, J. H., & Hook, S. C. (2005). Pitas Point anticline, California, USA, in: Shaw JH, Connors C, Suppe J (eds) Seismic interpretation of contractional fault-related folds. Am Assoc Pet Geol Seismic Atlas. Studies in Geology, 53, 60-62.

Singer, A., Beltrán C., and Rodríguez, J. A. (1998). Evidencias geomorfológicas de actividad neotectónica a lo largo de lor corrimientos frontales de la Serranía Del Interior en el oriente venezilano. 3rd. Geological Conference of the Geological Survey of Trinidad and Tobago.

Stephan, J. F. (1982). Evolution géodinamique du domaine Caraïbe, Andes et chaîne Caraibe sur la transversale de Barquisimeto (Vénézuéla) State. Thesis, Université Pierre et Marie Curie, Paris VI, France.

Stone, J. O. (2000). Air pressure and cosmogenic isotope production. Journal of Geophysical Research: Solid Earth (1978–2012), 105(B10), 23753-23759.

Summa, L., Goodman, E., Richardson, M., Norton, I., and Green, A. (2003). Hydrocarbon systems of Northeastern Venezuela: plate through molecular scale-analysis of the genesis and evolution of the Eastern Venezuela Basin. Marine and Petroleum Geology, 20(3), 323-349.

Suppe, J., Chou, G. T., and Hook, S. C. (1992). Rates of folding and faulting determined from growth strata.

Urbani, F., Hackley, P., Karlsen, A., and Garrity, C., 2005. Geological map of Venezuela: digital with shaded relief, scale 1:750.000. U.S. Geological Survey, Open-file report 2005-1038.

Vermeesch, P. (2007). CosmoCalc: An Excel add-in for cosmogenic nuclide calculations. Geochemistry, Geophysics, Geosystems, 8(8).

Wagner, R. (2004). Estudio Estructural Regional y Análisis de Deformaciones Recientes en el Frente de Montaña de La Serranía Del Interior Oriental y en la parte Norte de Subcuenca de Maturín. Unpublished undergrade work. Universidad Central de Venezuela, Caracas, Venezuela.

Weber, J. C., Dixon, T. H., DeMets, C., Ambeh, W. B., Jansma, P., Mattioli, G., and Pérez, O. (2001). GPS estimate of relative movement between the Caribbean and South American Plates, and geologic implications for Trinidad and Venezuela. Geology, 29(1), 75-78.

Zinck, J. A., and Urriola, P. L. (1970). Origen y evolución de la Formación Mesa. Un enfoque edafológico. Barcelona, Venezuela: Ministerio de Obras Públicas (MOP).